DIRECTION-PRESERVING ANCHOR LEARNING FOR MULTI-VIEW CLUSTERING

Anonymous authors
Paper under double-blind review

ABSTRACT

Anchor-based multi-view clustering commonly represents samples using orthogonal anchors and simplex-constrained assignment weights, and performs reconstruction with squared Euclidean distance. We identify an overlooked problem in this common formulation: under orthogonal anchors, the norm of the assignment vector directly determines the norm of the reconstructed sample. Since squared Euclidean loss depends on both direction and magnitude, the norm of the assignment weights also participates in minimizing the reconstruction error. As a result, the assignment weights, which are intended to describe clustering structure, are additionally influenced by reconstruction magnitude, interfering with the learning of the clustering representation. This additional influence may also hinder the clustering representation from adapting well to different numbers of anchors, making the model more sensitive to the anchor number. To address these problems, we propose Direction-Preserving Anchor Learning (DPAL), which normalizes each anchor combination before computing the reconstruction error. This preserves the representation direction determined by the assignment weights while making the reconstruction error independent of their norm. DPAL requires no additional regularization trade-off parameter and admits efficient closed-form alternating updates. Experiments on ten multi-view benchmark datasets show that DPAL substantially improves over conventional Euclidean reconstruction models, remains competitive with recent anchor-based methods, and is more stable with respect to the number of anchors.

1 INTRODUCTION

Multi-view clustering (MVC) seeks a common partition of aligned samples by integrating information distributed across heterogeneous views (Bickel & Scheffer, 2004; Xu et al., 2013; Zhou et al., 2024). Anchor-based MVC replaces dense sample–sample relations with a compact sample–anchor representation, reducing the graph size from $n \times n$ to $M \times n$ for $M \ll n$ (Chen & Cai, 2011; Liu et al., 2022; Wang et al., 2022b). A common formulation learns view-specific orthogonal anchors together with a shared nonnegative, sum-to-one assignment matrix and fits the samples by squared Euclidean reconstruction. Orthogonality controls anchor redundancy, the simplex constraint yields interpretable soft assignments, and Euclidean error provides a convenient reconstruction criterion. Recent methods retain this backbone and improve cluster-wise anchor organization (Zhang et al., 2024), introduce potential-cluster constraints (Chen et al., 2025), maximize Mahalanobis-guided separability (Zhang et al., 2025), calibrate anchors in dual spaces (Wang et al., 2026), or learn anchors in dual orthogonal spaces (Qin & Wu, 2026).

For sample i, the assignment vector z_i specifies how the anchors are combined and serves as its clustering representation. Under orthogonal anchors, however, $\|A^{(v)}z_i\|_2 = \|z_i\|_2$, meaning that the norm of the assignment vector directly determines the norm of the reconstructed sample. Since squared Euclidean loss depends on both direction and magnitude, changing $\|z_i\|_2$ also changes the reconstruction loss. Therefore, the norm of z_i participates in minimizing the reconstruction error, so the assignment weights used to describe clustering structure are also influenced by reconstruction magnitude.

Reviewers: please read the Reviewer Guidelines (iclr.cc/Conferences/2027/ReviewerGuidelines) and the AI Policy for Reviewers (iclr.cc/Conferences/2027/AIPolicyForReviewers). If you used AI to expand, edit, or polish your review, please provide the input text to the LLM. Better still, consider skipping the LLM and submitting your original text: we, and the authors, are much more interested in your unedited thoughts than in what an LLM has to say. AI-assisted or not, you are putting your name and reputation behind your review: LLM-generated falsehoods, hallucinations or misrepresentations are subject to disciplinary action, which may include desk-rejecting all papers you have authored.

This effect can be seen directly from the radial–angular decomposition. For input radius ρ, reconstruction scale r, and angular discrepancy θ,

$$\|y - Az\|_2^2 = (\rho - r)^2 + 2\rho r(1 - \cos\theta). \tag{1}$$

Here $r = \|z\|_2$. Both terms depend on the assignment norm. Thus, even when the representation direction is unchanged, changing $\|z\|_2$ changes the Euclidean reconstruction loss. The clustering representation is therefore affected not only by how the anchors represent the sample, but also by the reconstruction magnitude.

Increasing the number of anchors is generally expected to provide a richer representation space, allowing the model to describe the data using a larger set of anchors. However, Euclidean reconstruction imposes an additional restriction on how these anchors can be combined: the assignment weights must also produce a reconstruction norm that reduces the fitting error. As a result, an anchor combination that provides a useful representation direction may still be disfavored because of its reconstruction scale. This scale-fitting requirement can restrict the structural flexibility of the learned assignments, preventing the model from fully exploiting the additional anchors. Consequently, increasing the anchor number does not necessarily lead to a better clustering representation and may even cause substantial performance degradation. The problem is therefore not simply the number of available anchors, but how Euclidean reconstruction constrains their use through the assignment-controlled norm.

To remove this extra influence, we propose *Direction-Preserving Anchor Learning* (DPAL). Before evaluating the reconstruction error, DPAL normalizes each anchor combination as $Az/\|Az\|_2$. This operation preserves the representation direction selected by the assignment weights while making the reconstruction error independent of $\|z\|_2$. The assignment norm therefore no longer participates in reconstruction optimization, allowing the clustering representation to be learned according to the anchors without this additional influence. DPAL introduces no regularization trade-off coefficient and admits efficient closed-form alternating updates.

Our main contributions are summarized as follows:

- We identify an overlooked problem in Euclidean anchor reconstruction: under orthogonal anchors, the norm of the assignment weights directly determines the reconstruction norm and therefore participates in minimizing the Euclidean reconstruction error. This extra influence can interfere with representation learning and affect the clustering representations learned under different anchor numbers.
- We propose DPAL, which normalizes each anchor combination before reconstruction, preserving the represented direction while removing the influence of the assignment norm on the reconstruction error.
- We develop a closed-form alternating algorithm and establish monotonic objective decrease with linear complexity in the number of samples. Experiments on ten benchmarks demonstrate competitive clustering performance and reduced sensitivity to the number of anchors.

2 Related Work

2.1 Multi-view and Anchor-based Clustering

MVC methods exploit information agreement across heterogeneous views to obtain a unified partition (Bickel & Scheffer, 2004; Xu et al., 2013; Zhou et al., 2024). Traditional approaches learn common subspaces, consensus graphs, or compatible cluster assignments. Their sample-level graph construction limits scalability on large datasets. Landmark-based spectral clustering introduced a compact sample–landmark representation for reducing this burden (Chen & Cai, 2011). Subsequent anchor-based MVC methods jointly learn anchors and cross-view representations, including large-scale one-pass clustering (Liu et al., 2021), efficient one-pass consensus-anchor learning (Liu et al., 2022), and parameter-free consensus anchor guidance (Wang et al., 2022b).

Current research mainly improves the structure and coordination of anchors (Qiang et al., 2021; Wang et al., 2022a; Yu et al., 2024; Liu et al., 2024b; Qin et al., 2025; Wang et al., 2025). CAMVC organizes anchors according to cluster structure (Zhang et al., 2024); ALPC introduces potential-cluster constraints (Chen et al., 2025); MAGIC constructs anchors with diversity, balance, and com-

pactness through Max-Mahalanobis guidance (Zhang et al., 2025); DCMC couples the anchor and clustering spaces through dual calibration (Wang et al., 2026); and UEMCP learns common transition probabilities from data and anchors to categories in a probabilistic framework (Qin & Feng, 2026). Other developments enhance view correlation (Liu et al., 2024a), employ scalable tensor modeling (Long et al., 2024; Jia et al., 2026), capture individuality and commonality between anchor graphs (Lu et al., 2025), allocate anchors across clusters (Chen et al., 2026), or learn anchors in dual orthogonal spaces (Qin & Wu, 2026). These advances enrich anchor semantics and cross-view fusion. DPAL examines how the norm of the assignment weights affects squared Euclidean reconstruction under orthogonal anchors and simplex constraints.

3 METHODOLOGY

3.1 ASSIGNMENT NORM DETERMINES RECONSTRUCTION NORM

Let V be the number of views and n the number of aligned samples. The v-th raw feature matrix is $X^{(v)} = [x_1^{(v)}, \dots, x_n^{(v)}] \in \mathbb{R}^{d_v \times n}$. To distinguish the effect of input normalization from the reconstruction formulation, we consider two input protocols:

$$y_i^{(v)} = \begin{cases} x_i^{(v)}, & \text{original-input protocol,} \\ x_i^{(v)} / \|x_i^{(v)}\|_2, & \text{normalized-input protocol,} \end{cases} \qquad Y^{(v)} = [y_1^{(v)}, \dots, y_n^{(v)}]. \tag{2}$$

The model learns view-specific anchors $A^{(v)} \in \mathbb{R}^{d_v \times M}$ and a shared assignment matrix $Z = [z_1, \dots, z_n] \in \mathbb{R}^{M \times n}$ under

$$(A^{(v)})^\top A^{(v)} = I_M, \qquad Z \geq 0, \qquad \mathbf{1}^\top Z = \mathbf{1}^\top. \tag{3}$$

Orthogonality encourages nonredundant anchor directions. The simplex constraint makes each z_i an interpretable soft assignment. A standard Euclidean reconstruction formulation is

$$\min_{\{A^{(v)}\}, Z} \sum_{v=1}^{V} \left\| Y^{(v)} - A^{(v)} Z \right\|_F^2 \quad \text{s.t. (3).} \tag{4}$$

Proposition 1 (Assignment-controlled reconstruction scale)**.** *For every feasible z_i and every view, the representation-controlled reconstruction scale satisfies*

$$r_i^{(v)} = \|A^{(v)} z_i\|_2 = \|z_i\|_2, \qquad \frac{1}{\sqrt{M}} \leq r_i^{(v)} \leq 1. \tag{5}$$

If Z is shared, then $r_i^{(1)} = \cdots = r_i^{(V)}$.

Proof. Orthogonality gives $\|A^{(v)} z_i\|_2^2 = z_i^\top (A^{(v)})^\top A^{(v)} z_i = \|z_i\|_2^2$. For $z_i \geq 0$ and $\mathbf{1}^\top z_i = 1$, Cauchy–Schwarz gives $1 = (\mathbf{1}^\top z_i)^2 \leq M \|z_i\|_2^2$, and $\|z_i\|_2 \leq \|z_i\|_1 = 1$. The shared-radius statement follows because the same z_i is used in every view. □

The identity $\|A^{(v)} z_i\|_2 = \|z_i\|_2$ is the key result. The assignment vector z_i serves as the clustering representation of sample i, while under orthogonal anchors its norm directly determines the norm of the reconstructed sample. Therefore, changing the assignment weights changes both how the anchors represent the sample and the norm of the reconstruction.

3.2 ASSIGNMENT NORM IN EUCLIDEAN RECONSTRUCTION

Define the input radius $\rho_i^{(v)} = \|y_i^{(v)}\|_2$, the reconstruction radius $r_i = \|A^{(v)} z_i\|_2 = \|z_i\|_2$, and the angle $\theta_i^{(v)} = \angle(y_i^{(v)}, A^{(v)} z_i)$. Each Euclidean term decomposes exactly as

$$\begin{aligned} \left\| y_i^{(v)} - A^{(v)} z_i \right\|_2^2 &= (\rho_i^{(v)})^2 + r_i^2 - 2\rho_i^{(v)} r_i \cos\theta_i^{(v)} \\ &= \underbrace{(\rho_i^{(v)} - r_i)^2}_{\text{scale matching}} + \underbrace{2\rho_i^{(v)} r_i (1 - \cos\theta_i^{(v)})}_{\text{scale-weighted angular mismatch}}. \end{aligned} \tag{6}$$

Equation 6 shows that the assignment norm $r_i = \|z_i\|_2$ directly affects the Euclidean reconstruction loss. The assignment weights used for clustering are therefore influenced not only by how the anchors represent the sample, but also by their effect on the reconstruction norm.

For fixed reconstructed directions, the sample-wise loss is

$$L_i(r_i) = C_i + Vr_i^2 - 2r_i \sum_{v=1}^{V} \rho_i^{(v)} \cos\theta_i^{(v)}, \qquad C_i = \sum_{v=1}^{V} (\rho_i^{(v)})^2. \tag{7}$$

Proposition 2 (Radial relaxation of Euclidean reconstruction)**.** *For fixed reconstructed directions, treating r_i as an independent scalar gives the unconstrained minimizer of equation 7:*

$$r_{i,\text{target}} = \frac{1}{V} \sum_{v=1}^{V} \rho_i^{(v)} \cos\theta_i^{(v)}. \tag{8}$$

After enforcing the simplex-induced interval, its radial relaxation is

$$r_i^{\dagger} = \Pi_{[1/\sqrt{M},\,1]} \left(\frac{1}{V} \sum_{v=1}^{V} \rho_i^{(v)} \cos\theta_i^{(v)} \right). \tag{9}$$

Proof. Differentiating equation 7 gives $2Vr_i - 2\sum_v \rho_i^{(v)} \cos\theta_i^{(v)}$. Setting it to zero yields equation 8; projection onto the feasible interval gives equation 9. □

Proposition 2 characterizes the scale preferred by Euclidean reconstruction. In the original simplex-constrained problem, the assignment norm and representation direction are coupled, so the relaxed optimum need not be attainable at a fixed direction. Nevertheless, the loss favors feasible assignments whose norms better match this preferred scale, thereby influencing the learned representation.

For each choice of M, the clustering representation should reflect the corresponding number of anchors. Because $\|z_i\|_2$ also participates in the Euclidean reconstruction loss, the learned representation is additionally influenced by the reconstruction norm. This extra influence can hinder how well the clustering representation fits the chosen anchor number and makes the model more sensitive to M.

3.3 Direction-Preserving Anchor Learning

The analysis above shows that the assignment norm directly participates in Euclidean reconstruction optimization. DPAL removes this influence by normalizing each nonzero anchor combination before computing the reconstruction error:

$$\widehat{y}_i^{(v)} = \frac{A^{(v)} z_i}{\|A^{(v)} z_i\|_2} = \frac{A^{(v)} z_i}{\|z_i\|_2}. \tag{10}$$

This normalization preserves the representation direction determined by $A^{(v)} z_i$, while removing its norm from the reconstruction comparison. The reconstruction error therefore becomes independent of $\|z_i\|_2$, so the assignment norm no longer participates in reconstruction optimization. The proposed model is

$$\min_{\{A^{(v)}\},Z} F = \sum_{v=1}^{V} \sum_{i=1}^{n} \left\| y_i^{(v)} - \widehat{y}_i^{(v)} \right\|_2^2 \quad \text{s.t. (3)}. \tag{11}$$

Using the same input radius and angular notation,

$$\left\| y_i^{(v)} - \widehat{y}_i^{(v)} \right\|_2^2 = (\rho_i^{(v)} - 1)^2 + 2\rho_i^{(v)}(1 - \cos\theta_i^{(v)}). \tag{12}$$

The first term is independent of $A^{(v)}$ and Z. Original inputs weight each angular error by $\rho_i^{(v)}$, while normalized inputs assign unit weight to every angular error. Equation 12 shows that the optimization-dependent reconstruction loss contains no $r_i = \|z_i\|_2$. The assignment weights therefore determine the represented direction without their norm additionally affecting the reconstruction error.

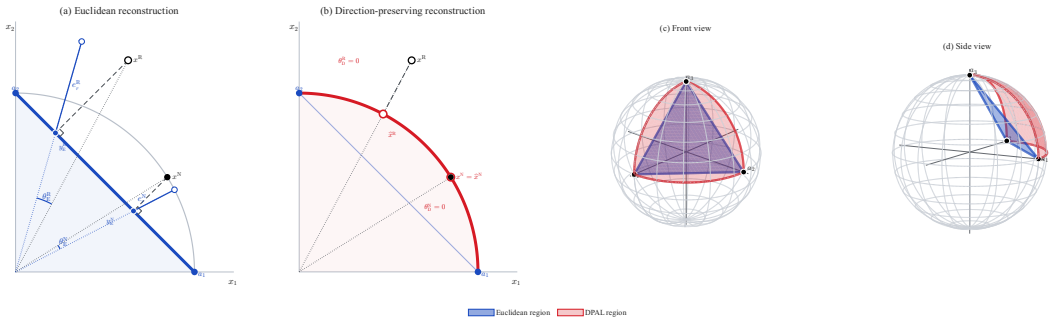

Figure 1: Assignment norm in anchor reconstruction. (a)–(b) Euclidean reconstruction is affected by both the represented direction and the assignment-controlled reconstruction norm. DPAL preserves the direction of each anchor combination while removing the influence of its norm from the reconstruction loss. (c)–(d) Front and side views of the Euclidean planar simplex (blue) and its radially projected hyperspherical region (red).

For each choice of M, DPAL learns the clustering representation from the corresponding anchors. Because the assignment norm is absent from the reconstruction loss, the representation is no longer additionally influenced by its norm during reconstruction optimization.

Figure 1 summarizes the difference between Euclidean reconstruction and DPAL. Under Euclidean reconstruction, the assignment norm directly affects the reconstruction loss. DPAL normalizes the anchor combination before comparison, preserves its representation direction, and removes the influence of the assignment norm from reconstruction optimization. With three orthogonal anchors, the projection maps the planar Euclidean simplex to its corresponding hyperspherical patch.

3.4 Closed-form Alternating Optimization

Define the column-normalized representation

$$q_i = \frac{z_i}{\|z_i\|_2}, \qquad Q = [q_1, \ldots, q_n]. \tag{13}$$

After discarding constants, minimizing equation 11 is equivalent to maximizing $\sum_v \mathrm{Tr}((A^{(v)})^\top Y^{(v)} Q^\top)$. We optimize the two variable blocks alternately.

Updating $A^{(v)}$. With Z fixed, the views are separable and the v-th anchor subproblem is

$$\max_{(A^{(v)})^\top A^{(v)} = I_M} \mathrm{Tr}\Big((A^{(v)})^\top Y^{(v)} Q^\top\Big). \tag{14}$$

Let the compact singular value decomposition be

$$Y^{(v)} Q^\top = U^{(v)} \Sigma^{(v)} (R^{(v)})^\top. \tag{15}$$

Equation 14 is an orthogonal Procrustes problem, whose global solution is

$$A^{(v)} \leftarrow U^{(v)} (R^{(v)})^\top. \tag{16}$$

Updating Z. With all anchors fixed, the columns of Z are independent. Define the cross-view directional correlation

$$c_i = \sum_{v=1}^{V} (A^{(v)})^\top y_i^{(v)}. \tag{17}$$

Using $q_i = z_i / \|z_i\|_2$, each subproblem becomes

$$\max_{q_i \geq 0,\ \|q_i\|_2 = 1} c_i^\top q_i. \tag{18}$$

Let $[c_i]_+ = \max(c_i, 0)$ element-wise. If $[c_i]_+ \neq 0$, the Cauchy–Schwarz inequality gives $q_i = [c_i]_+ / \|[c_i]_+\|_2$. Mapping it back to the simplex yields

$$z_i \leftarrow \frac{[c_i]_+}{\mathbf{1}^\top [c_i]_+}. \tag{19}$$

If $[c_i]_+ = 0$, the solution is the one-hot vector associated with the largest entry of c_i.

Algorithm 1 Direction-Preserving Anchor Learning

Require: Supplied multi-view inputs $\{Y^{(v)}\}_{v=1}^{V}$ from either protocol in equation 2, anchor number M, maximum iteration T, and tolerance ε.
Ensure: Assignment matrix Z.
1: Initialize each $A^{(v)}$ with orthonormal columns and initialize a feasible $Z \geq 0$ with $\mathbf{1}^\top Z = \mathbf{1}^\top$.
2: **repeat**
3: Normalize the columns of Z to obtain Q by equation 13.
4: Update every $A^{(v)}$ by equations 15–16.
5: Compute c_i by equation 17 and update every z_i by equation 19.
6: **until** the maximum iteration is reached or $|F^{(t)} - F^{(t-1)}| < \varepsilon$.

3.5 Convergence and Complexity Analysis

Proposition 3 (Monotonic decrease)**.** *Let $F^{(t)}$ be the value of equation 11 after iteration t of Algorithm 1. Then $F^{(t+1)} \leq F^{(t)}$, and the resulting objective sequence converges.*

Proof. For fixed Z, equation 16 globally solves each orthogonal Procrustes subproblem. For fixed $\{A^{(v)}\}$, equation 19 globally solves each independent representation subproblem. Therefore neither block update can increase F. Moreover, every summand of equation 11 is nonnegative, so $F \geq 0$. The sequence is thus monotonically nonincreasing and lower bounded, which proves convergence. □

The dominant operations are forming $Y^{(v)}Q^\top$, evaluating the correlations in equation 17, and computing an SVD of a $d_v \times M$ matrix for each view. The per-iteration time complexity is

$$\mathcal{O}\left(nM\sum_{v=1}^{V} d_v + M^2\sum_{v=1}^{V} d_v\right), \tag{20}$$

which is linear in n when M and V are small. Storing the data and the assignment matrix requires $\mathcal{O}(n\sum_v d_v + nM)$ memory, apart from the comparatively small anchor matrices.

4 Experiments

4.1 Experimental Setup

We evaluate DPAL on ten public multi-view benchmarks covering text, image, image–text, and video data. Their statistics are summarized in Table 1.

Table 1: Statistics of the current benchmark datasets.

Dataset	Samples	Views	Classes	Type	Dataset	Samples	Views	Classes	Type
3Sources	169	3	6	Text	COIL20	1,440	3	20	Image
MSRC	210	5	7	Image	Wiki	2,866	2	10	Image–text
NGs	500	3	5	Text	Notting-Hill	4,660	3	5	Video
BBCSport	544	2	5	Text	Fashion	10,000	3	10	Image
Reuters	1,200	5	6	Text	MNIST-f	60,000	3	10	Image

We compare with five recent anchor-based MVC methods, CAMVC (Zhang et al., 2024), ALPC (Chen et al., 2025), MAGIC (Zhang et al., 2025), DCMC (Wang et al., 2026), and UEMCP (Qin & Feng, 2026), together with the matched Euclidean baseline in equation 4. Released implementations are used when available, with method-specific hyperparameters selected from the recommended ranges. For DPAL and its controlled variants, the anchor number is selected from $M \in \{k, 2k, 3k, 4k, 5k\}$, where k is the number of clusters; the largest feasible value is used when the feature dimension limits the orthogonal-anchor constraint. Each model is independently trained 20 times. Each learned representation is evaluated by 30 single-start k-means runs, retaining the run with the highest ACC, and the mean over the 20 model runs is reported. We report ACC, NMI, ARI, and Purity. All experiments are conducted in MATLAB R2025b on Windows 11 with an Intel Core i7-14700F CPU and 16 GB RAM.

Table 2: Mean clustering results (%) over 20 independent model runs. Each cell reports ACC/NMI and ARI/Purity. For competing methods, superscripts O and N denote original and sample-wise normalized inputs, respectively. The best result is in bold and the second best is underlined.

Dataset	CAMVC (AAAI 2024)	ALPC (AAAI 2025)	MAGIC (AAAI 2025)	UEMCP (ICLR 2026)	DCMC (ICML 2026)	DPAL-O (Ours)	DPAL-N (Ours)
3Sources	77.46/68.58 62.03/81.51^{N}	74.41/68.33 59.73/82.25^{N}	73.37/65.70 64.33/79.29^{N}	63.43/57.54 47.33/72.25^{N}	81.33/71.31 67.25/84.35^{N}	**86.24/76.01** **75.14/87.87**	82.19/73.84 70.12/85.95
BBCSport	93.25/82.34 83.00/93.25^{O}	92.97/80.22 82.39/92.97^{O}	89.52/75.36 78.90/89.52^{N}	81.07/73.41 67.52/80.17^{N}	94.72/85.12 85.80/94.72^{O}	**94.81/85.44** **85.83/94.81**	94.23/84.30 85.00/94.23
MSRC	85.71/76.43 73.03/85.71^{N}	86.64/77.65 72.70/86.64^{N}	82.86/71.60 63.26/82.86^{N}	70.36/61.23 50.00/71.40^{N}	86.19/76.87 72.08/86.67^{N}	59.10/47.15 33.61/60.55	**87.79/78.45** **73.57/87.79**
Fashion	75.11/76.17 67.42/75.66^{O}	77.43/73.55 63.15/77.60^{O}	75.65/74.38 64.17/75.92^{N}	69.63/74.14 57.84/72.96^{N}	79.65/74.25 65.62/79.68^{O}	**82.29**/78.96 70.77/82.29	81.90/**79.96** **71.52/82.66**
Notting-Hill	84.41/75.31 76.22/84.71^{O}	93.51/87.65 88.26/93.51^{N}	88.13/75.00 79.13/88.13^{O}	47.57/28.99 21.68/47.61^{O}	84.57/74.42 75.10/84.92^{O}	85.33/76.48 76.91/85.74	**94.78/90.21** **90.41/94.78**
NGs	98.19/93.25 95.52/98.19^{N}	98.00/93.79 95.03/98.00^{N}	97.60/92.17 94.26/97.60^{N}	31.66/14.77 13.75/32.17^{N}	98.15/94.19 95.34/98.18^{N}	96.90/90.59 92.36/96.90	**98.25/94.32** **95.65/98.25**
Reuters	65.33/42.96 35.84/65.37^{N}	**65.60**/43.05 **36.45/65.60**^{N}	55.42/34.05 32.57/55.42^{N}	37.97/15.41 12.23/38.93^{O}	63.92/43.06 35.45/63.76^{O}	64.11/42.73 35.42/64.11	64.67/**43.33** 35.79/64.67
COIL20	74.38/83.08 67.76/75.14^{O}	**74.44/83.32** **67.89/75.76**^{O}	68.67/44.86 40.95/68.67^{N}	71.26/80.17 63.32/71.98^{O}	71.88/80.47 63.43/73.12^{O}	73.54/82.04 67.36/75.49	70.26/79.62 62.35/70.69
Wiki	60.43/54.52 46.71/62.91^{O}	**61.21/56.26** **48.96/64.48**^{O}	59.28/52.44 45.23/62.11^{N}	28.89/16.67 12.92/29.44^{O}	59.69/54.23 44.76/60.54^{O}	60.62/54.98 47.04/63.19	58.93/50.72 43.53/61.24
MNIST-f	**99.10/97.23** **98.01/99.10**^{O}	99.00/96.92 97.80/99.00^{O}	97.68/94.36 95.57/97.51^{O}	30.58/45.84 17.70/30.59^{O}	98.51/95.70 96.72/98.51^{O}	99.04/97.06 97.87/99.04	98.58/95.98 96.88/98.58

4.2 Comparison with Anchor-based MVC Methods

Each competing method is evaluated on both the original and sample-wise normalized inputs, and the input yielding the highest retained ACC is reported. DPAL-O and DPAL-N denote the original- and normalized-input protocols in equation 2, respectively, and both use the projected reconstruction in equation 10. Table 2 reports the clustering results.

On the first six benchmarks, DPAL achieves the best ACC and NMI results, demonstrating particularly strong clustering performance. On the remaining four benchmarks, although DPAL does not attain the highest scores, its results remain close to those of the best-performing methods. More importantly, DPAL involves only the anchor number M as its model-selection parameter, whereas the compared methods require method-specific hyperparameters to be tuned separately for different datasets. The anchor-number experiments in Figure 4 show that DPAL maintains stable performance over a broad range of anchor numbers. Considering both clustering performance and model-selection complexity, DPAL therefore demonstrates strong overall competitiveness across the ten benchmarks.

4.3 Efficiency and Convergence

Figure 2 compares model-function time under normalized inputs, matched anchor numbers, and matched iterations. Preprocessing, diagnostics, and final k-means are excluded from the timing.

Across the ten benchmarks, DPAL remains within the low running-time range of the efficient anchor-based methods.

Figure 3 reports the objective value and ACC over iterations on all ten benchmarks.

The objective decreases rapidly and reaches a stable value within a small number of iterations, while the ACC curves stabilize accordingly. This empirical behavior is consistent with the monotonic objective decrease established in Proposition 3.

4.4 Controlled Analysis and Anchor-Number Behavior

The four variants in Table 3 separate the effect of input normalization from the effect of removing the assignment norm from the reconstruction loss. Original-Euc and Normalized-Euc use the same Euclidean reconstruction on original and sample-wise normalized inputs, respectively. DPAL-O and DPAL-N use the proposed reconstruction under the corresponding two input protocols.

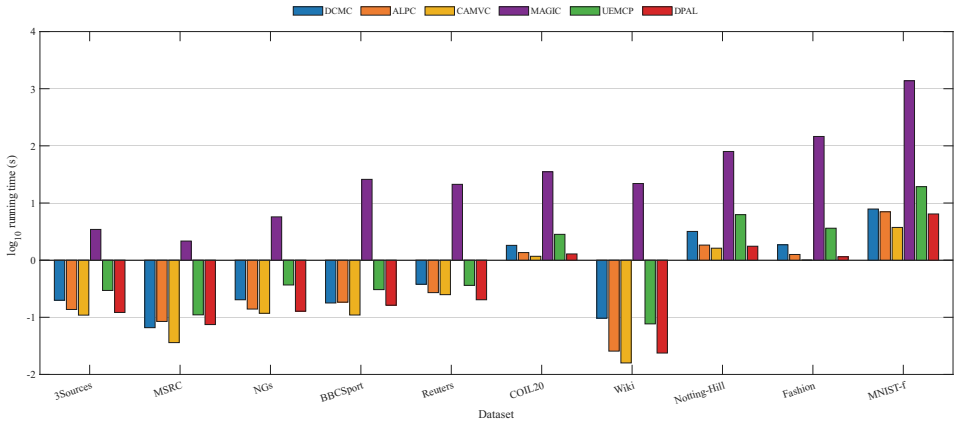

Figure 2: Controlled model-function running time on ten normalized-input benchmarks.

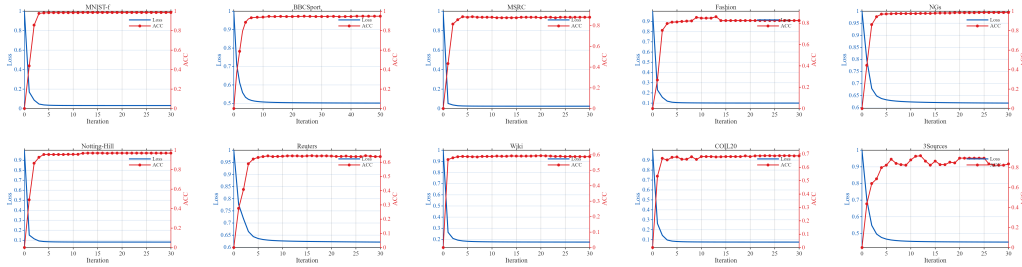

Figure 3: Objective values and ACC over iterations on ten benchmarks.

Table 3: Controlled ACC/NMI results (%, mean ± standard deviation over 20 independent model runs). O and N denote the original- and normalized-input protocols, respectively.

Dataset	Original-Euc	Normalized-Euc	DPAL-O	DPAL-N
3Sources	65.83±6.48/48.26±5.81	79.62±4.94/69.41±5.13	**86.24±4.44/76.01±3.30**	82.19±4.63/73.84±2.72
BBCSport	73.19±12.23/56.13±13.03	94.10±0.47/83.78±1.18	**94.81±0.35/85.44±0.90**	94.23±0.82/84.30±1.24
MSRC	14.76±0.00/5.48±0.00	75.48±2.99/68.03±3.13	59.10±1.53/47.15±1.43	**87.79±0.23/78.45±0.44**
Fashion	18.10±0.45/22.10±0.34	74.72±1.99/75.80±1.60	**82.29±1.05**/78.96±0.44	81.90±1.97/**79.96±0.60**
NGs	84.90±7.22/72.85±8.41	98.19±0.28/94.03±0.75	96.90±0.45/90.59±1.19	**98.25±0.24/94.32±0.77**
Notting-Hill	30.11±0.00/0.16±0.00	84.39±3.57/74.98±5.53	85.33±2.26/76.48±2.59	**94.78±2.43/90.21±3.43**
Reuters	38.83±5.89/26.83±5.53	64.08±0.88/43.13±1.21	64.11±1.11/42.73±1.00	**64.67±0.59/43.33±1.30**
Wiki	60.25±0.16/54.55±0.31	58.64±0.96/49.03±0.62	**60.62±0.16/54.98±0.18**	58.93±0.44/50.72±0.14
COIL20	71.07±2.15/81.48±1.21	68.64±2.47/78.95±1.40	**73.54±2.32/82.04±1.25**	70.26±2.77/79.62±1.26
MNIST-f	**99.07±0.00/97.15±0.00**	97.81±0.48/94.62±0.75	99.04±0.00/97.06±0.00	98.58±0.00/95.98±0.00

Table 3 shows a clear and consistent effect of the proposed reconstruction. Under normalized inputs, DPAL-N improves both ACC and NMI over Normalized-Euc on all ten datasets. Under original inputs, DPAL-O improves both metrics over Original-Euc on nine datasets, while MNIST-f remains nearly unchanged. The improvements are particularly large on several datasets, including MSRC, Fashion, and Notting-Hill. These results show that the performance gain comes from the reconstruction itself rather than from input normalization alone. After fixing the input protocol, removing the influence of the assignment norm from the reconstruction loss consistently improves the learned clustering representation.

Figure 4 compares the four controlled variants over the complete anchor-number range on eight datasets. Original-Euc is highly sensitive to the anchor number on several benchmarks, with clustering accuracy changing substantially as M increases. Sample-wise normalization clearly mitigates this instability, but does not eliminate it: Normalized-Euc still exhibits noticeable changes over M on multiple datasets. In contrast, DPAL-O and DPAL-N remain stable over broad anchor-number ranges. Since each DPAL variant is compared with its Euclidean counterpart under exactly the same input protocol, this difference shows that the improved stability originates from removing assignment-norm fitting rather than from input normalization alone.

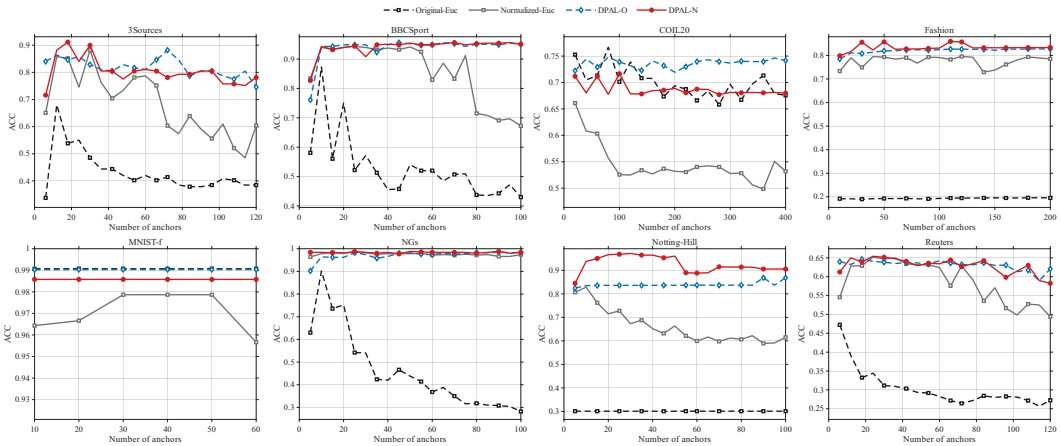

Figure 4: ACC versus the number of anchors for the four controlled variants on 3Sources, BBCSport, COIL20, Fashion, MNIST-f, NGs, Notting-Hill, and Reuters.

Figure 5 provides the corresponding representation-level explanation. For a simplex-constrained assignment, $\|z_i\|_2$ ranges from $1/\sqrt{M}$ for a uniform assignment to 1 for a one-hot assignment; a larger norm therefore indicates a more concentrated use of the available anchors. Original-Euc maintains high mean assignment norms on most benchmarks, indicating that its representations remain concentrated on a small subset of anchors even as M grows. Normalization lowers this concentration and partially improves the behavior, but the assignment norm still does not consistently adapt to the enlarged anchor set. Thus, increasing the number of available anchors does not necessarily translate into a correspondingly richer Euclidean clustering representation.

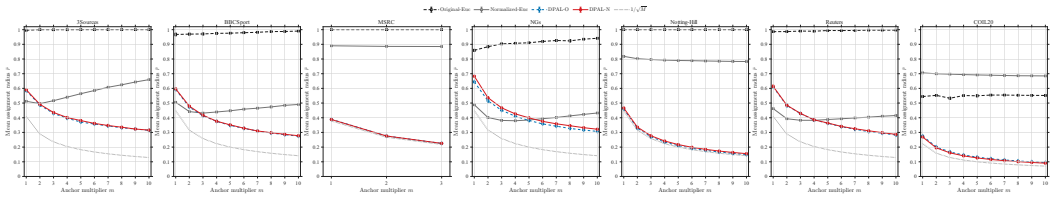

Figure 5: Mean assignment norm versus the anchor multiplier for the four controlled variants on seven benchmarks.

DPAL exhibits a different response. Once the assignment norm is removed from the reconstruction loss, it is no longer optimized for reconstruction-scale matching and can change according to the available anchor structure. The assignments consequently make broader use of the anchor set as M increases, which is further confirmed by the effective-anchor-number and anchor-usage diagnostics in Appendix A. Figures 4 and 5 connect the theoretical analysis with the observed sensitivity: Euclidean reconstruction couples structural assignment with scale fitting, normalization weakens this coupling, and DPAL removes it to obtain stronger anchor-number stability.

5 Conclusion

This paper shows that, under orthogonal anchors, the assignment weights used for clustering also determine the reconstruction norm. Their norm therefore participates directly in squared Euclidean reconstruction and can additionally influence the learned clustering representation. DPAL normalizes each anchor combination before reconstruction and makes the reconstruction error independent of the assignment norm. Its coefficient-free objective admits efficient closed-form alternating updates. Experiments on ten multi-view benchmarks show consistent improvements over matched Euclidean baselines, competitive performance against recent anchor-based methods, and reduced sensitivity to the number of anchors.

AI USE STATEMENT

Generative AI tools were used to assist with language refinement, the refinement and checking of mathematical derivations, code drafting, experimental planning and result interpretation, and the preparation of figures and tables. All AI-assisted mathematical claims and derivations were independently checked by the authors; all generated or modified code was executed and validated; and all numerical results, figures, tables, citations, and conclusions were verified against the authors' experimental outputs and source materials. The authors made all final methodological and interpretive decisions and take full responsibility for the final content of the work.

REFERENCES

Steffen Bickel and Tobias Scheffer. Multi-view clustering. In *Proceedings of the IEEE International Conference on Data Mining*, pp. 19–26, 2004. doi: 10.1109/ICDM.2004.10095.

Xinlei Chen and Deng Cai. Large scale spectral clustering with landmark-based representation. In *Proceedings of the AAAI Conference on Artificial Intelligence*, volume 25, pp. 313–318, 2011. doi: 10.1609/aaai.v25i1.7900.

Yawei Chen, Huibing Wang, Jinjia Peng, and Yang Wang. Anchor learning with potential cluster constraints for multi-view clustering. In *Proceedings of the AAAI Conference on Artificial Intelligence*, pp. 15939–15947, 2025. doi: 10.1609/aaai.v39i15.33750.

Zhe Chen, Fanhui Meng, Tianyang Xu, and Xiao-Jun Wu. Cluster-aware anchor learning for multi-view clustering. In *Proceedings of the IEEE/CVF Conference on Computer Vision and Pattern Recognition*, pp. 17714–17723, 2026.

Miao Jia, Xingchen Hu, Jiyuan Liu, Siwei Wang, Min Wang, and Zijian Chen. Scalable multi-view subspace clustering with tensorized anchor guidance. In *Proceedings of the IEEE/CVF Conference on Computer Vision and Pattern Recognition*, pp. 14367–14374, 2026.

Jiyuan Liu, Xinwang Liu, Yuexiang Yang, Li Liu, Siqi Wang, Weixuan Liang, and Jiangyong Shi. One-pass multi-view clustering for large-scale data. In *Proceedings of the IEEE/CVF International Conference on Computer Vision*, pp. 12344–12353, 2021.

Suyuan Liu, Siwei Wang, Pei Zhang, Kai Xu, Xinwang Liu, Changwang Zhang, and Feng Gao. Efficient one-pass multi-view subspace clustering with consensus anchors. In *Proceedings of the AAAI Conference on Artificial Intelligence*, pp. 7576–7584, 2022. doi: 10.1609/aaai.v36i7.20723.

Suyuan Liu, Ke Liang, Zhibin Dong, Siwei Wang, Xihong Yang, Sihang Zhou, En Zhu, and Xinwang Liu. Learn from view correlation: An anchor enhancement strategy for multi-view clustering. In *Proceedings of the IEEE/CVF Conference on Computer Vision and Pattern Recognition*, pp. 26151–26161, 2024a.

Suyuan Liu, Qing Liao, Siwei Wang, Xinwang Liu, and En Zhu. Robust and consistent anchor graph learning for multi-view clustering. *IEEE Transactions on Knowledge and Data Engineering*, 36 (8):4207–4219, 2024b. doi: 10.1109/TKDE.2024.3364663.

Zhen Long, Qiyuan Wang, Yazhou Ren, Yipeng Liu, and Ce Zhu. S2MVTC: A simple yet efficient scalable multi-view tensor clustering. In *Proceedings of the IEEE/CVF Conference on Computer Vision and Pattern Recognition*, pp. 26213–26222, 2024.

Zhoumin Lu, Yongbo Yu, Linru Ma, Feiping Nie, and Rong Wang. Capturing individuality and commonality between anchor graphs for multi-view clustering. In *Proceedings of the International Joint Conference on Artificial Intelligence*, pp. 5860–5868, 2025. doi: 10.24963/ijcai.2025/652.

Qianyao Qiang, Bin Zhang, Fei Wang, and Feiping Nie. Fast multi-view discrete clustering with anchor graphs. In *Proceedings of the AAAI Conference on Artificial Intelligence*, volume 35, pp. 9360–9367, 2021. doi: 10.1609/aaai.v35i11.17128.

Yalan Qin and Guorui Feng. Unified and efficient multi-view clustering from probabilistic perspective. In *International Conference on Learning Representations*, 2026.

Yalan Qin and Hanzhou Wu. Learning anchor in dual orthogonal space for fast multi-view clustering. In *Proceedings of the IEEE/CVF Conference on Computer Vision and Pattern Recognition*, pp. 1616–1626, 2026.

Yalan Qin, Nan Pu, Guorui Feng, and Nicu Sebe. Robust consensus anchor learning for efficient multi-view subspace clustering. In *Proceedings of the 42nd International Conference on Machine Learning*, volume 267 of *Proceedings of Machine Learning Research*, pp. 50327–50337, 2025.

Bocheng Wang, Chusheng Zeng, Mulin Chen, and Xuelong Li. Towards learnable anchor for deep multi-view clustering. In *Proceedings of the AAAI Conference on Artificial Intelligence*, volume 39, pp. 21044–21052, 2025. doi: 10.1609/aaai.v39i20.35401.

Huibing Wang, Yuemeng Huang, Yawei Chen, Jiaxin Yang, Qian Liu, Jinjia Peng, Zetian Mi, and Ximing Li. Dual-calibration multi-view clustering via compact anchor learning. In *Proceedings of the International Conference on Machine Learning*, 2026.

Siwei Wang, Xinwang Liu, Suyuan Liu, Jiaqi Jin, Wenxuan Tu, Xinzhong Zhu, and En Zhu. Align then fusion: Generalized large-scale multi-view clustering with anchor matching correspondences. In *Advances in Neural Information Processing Systems*, volume 35, pp. 5882–5895, 2022a.

Siwei Wang, Xinwang Liu, Xinzhong Zhu, Pei Zhang, Yi Zhang, Feng Gao, and En Zhu. Fast parameter-free multi-view subspace clustering with consensus anchor guidance. *IEEE Transactions on Image Processing*, 31:556–568, 2022b. doi: 10.1109/TIP.2021.3131941.

Chang Xu, Dacheng Tao, and Chao Xu. A survey on multi-view learning. *arXiv preprint arXiv:1304.5634*, 2013.

Shengju Yu, Siwei Wang, Pei Zhang, Miao Wang, Ziming Wang, Zhe Liu, Liming Fang, En Zhu, and Xinwang Liu. DVSAI: Diverse view-shared anchors based incomplete multi-view clustering. In *Proceedings of the AAAI Conference on Artificial Intelligence*, volume 38, pp. 16568–16577, 2024. doi: 10.1609/aaai.v38i15.29595.

Chao Zhang, Xiuyi Jia, Zechao Li, Chunlin Chen, and Huaxiong Li. Learning cluster-wise anchors for multi-view clustering. In *Proceedings of the AAAI Conference on Artificial Intelligence*, pp. 16696–16704, 2024. doi: 10.1609/aaai.v38i15.29609.

Pei Zhang, Yuangang Pan, Siwei Wang, Shengju Yu, Huiying Xu, En Zhu, Xinwang Liu, and Ivor Tsang. Max-Mahalanobis anchors guidance for multi-view clustering. In *Proceedings of the AAAI Conference on Artificial Intelligence*, pp. 22488–22496, 2025. doi: 10.1609/aaai.v39i21.34406.

Lihua Zhou, Guowang Du, Kevin Lü, Lizhen Wang, and Jingwei Du. A survey and an empirical evaluation of multi-view clustering approaches. *ACM Computing Surveys*, 56(7):187:1–187:38, 2024. doi: 10.1145/3645108.

A Additional Experimental Diagnostics

A.1 Additional Anchor-Usage Distributions

For an assignment matrix Z, let $u_j = \sum_{i=1}^{n} Z_{ji}$ denote the total assignment weight received by anchor j, let $p_j = u_j / \sum_{\ell=1}^{M} u_\ell$ with the convention $0 \log 0 = 0$, and let $\bar{u} = M^{-1} \sum_{j=1}^{M} u_j$. We quantify anchor utilization by

$$N_{\text{eff}} = \exp\left(-\sum_{j=1}^{M} p_j \log p_j \right), \qquad \text{CV} = \frac{\sqrt{\frac{1}{M-1} \sum_{j=1}^{M} (u_j - \bar{u})^2}}{\bar{u}}. \tag{21}$$

A larger N_{eff} (at most M) indicates that more anchors are effectively used, whereas a smaller CV indicates a more balanced assignment.

The following plots show the total assignment weight received by each anchor. Isolated high bars indicate concentration on a small subset, whereas comparable bar heights indicate broader use of the learned anchor set.

Figure 6 tracks each controlled variant on COIL20 across anchor multipliers from 1 to 4. The two Euclidean variants place progressively more assignment mass on a few anchors, whereas DPAL-O and DPAL-N maintain broader use throughout the same sequence.

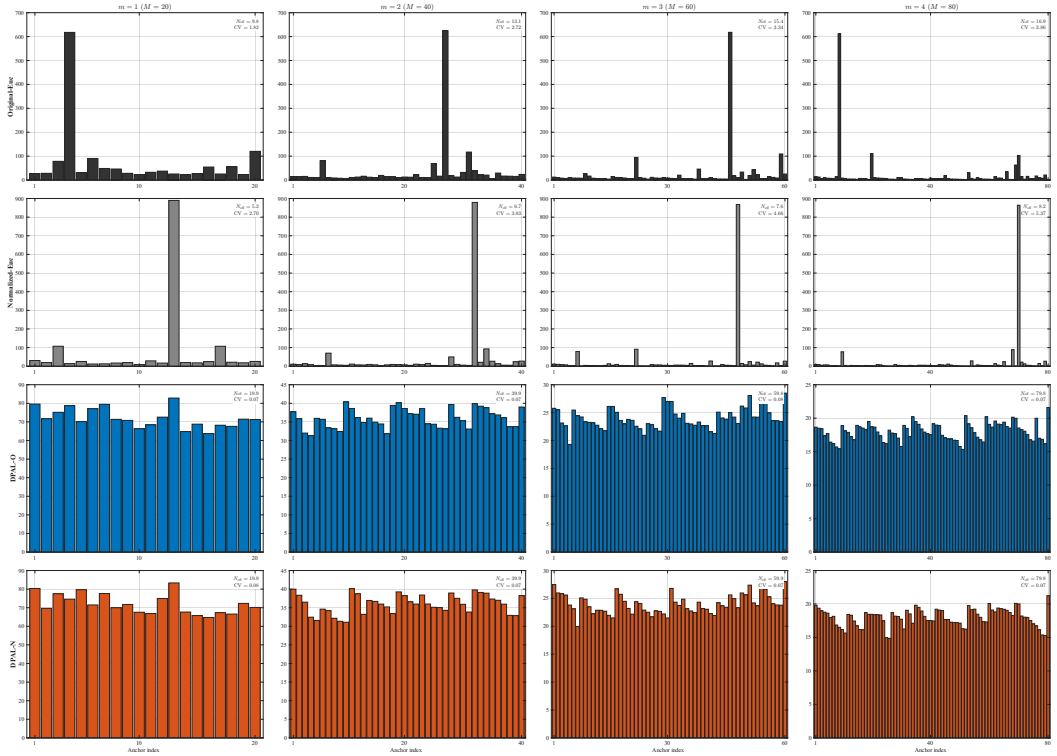

Figure 6: Anchor-usage progression on COIL20. Each row fixes one reconstruction variant. Columns increase the anchor multiplier from $m = 1$ to $m = 4$.

Figure 7 compares the four controlled variants on BBCSport and NGs at the selected anchor setting. Figures 8–11 then extend the analysis to eight additional benchmarks. The actual anchor number M is reported in every panel.

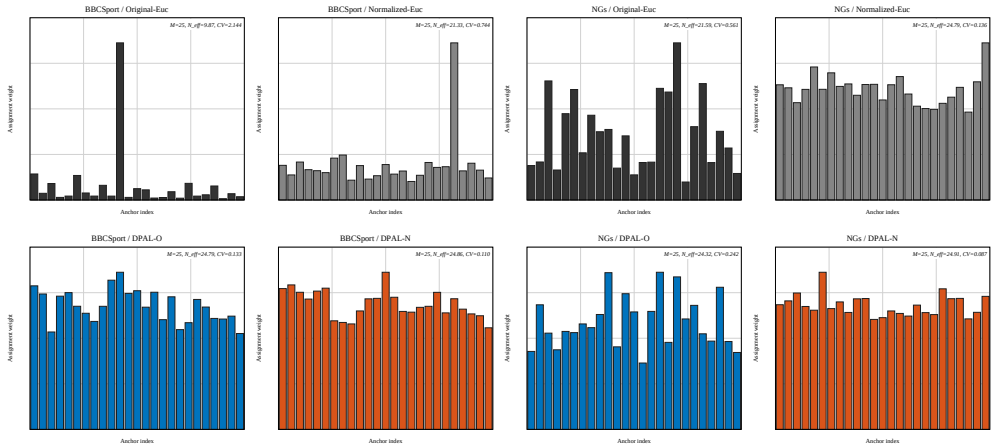

Figure 7: Anchor-usage distributions on BBCSport (left two columns) and NGs (right two columns), with Euclidean variants in the top row and DPAL variants in the bottom row.

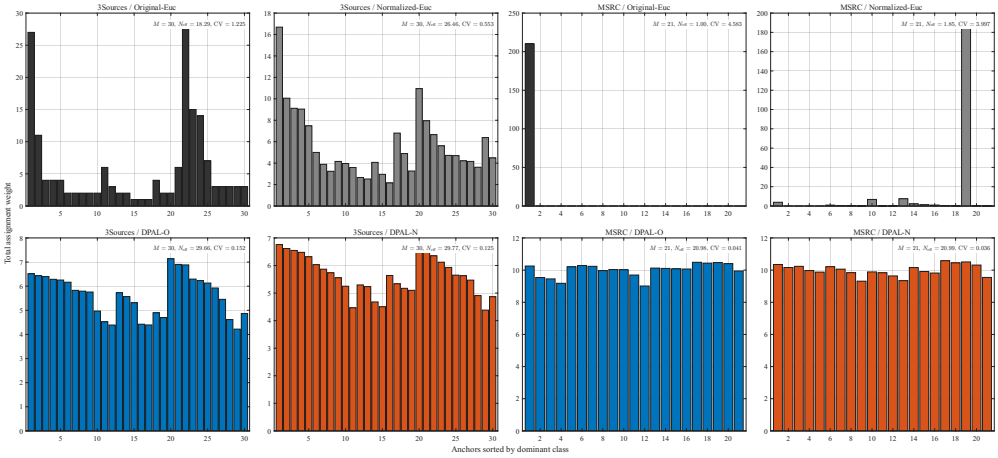

Figure 8: Anchor-usage distributions of the four controlled variants on 3Sources and MSRC.

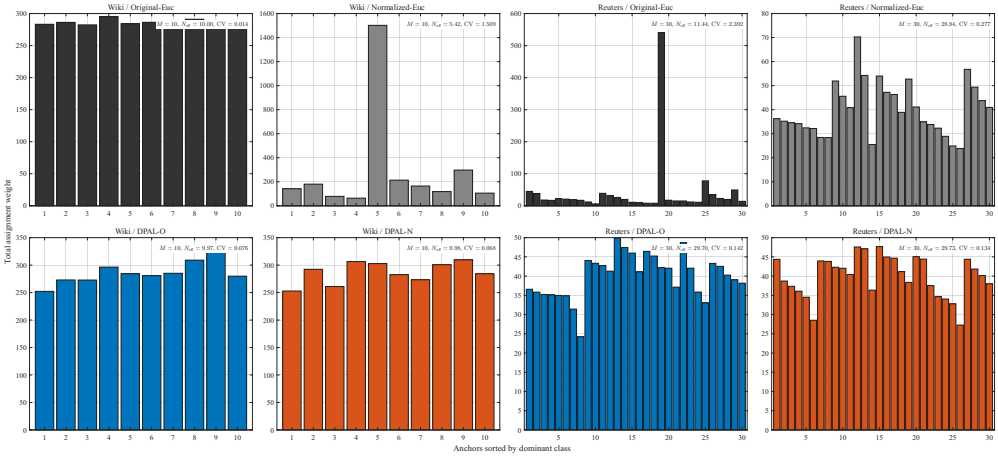

Figure 9: Anchor-usage distributions of the four controlled variants on Wiki and Reuters.

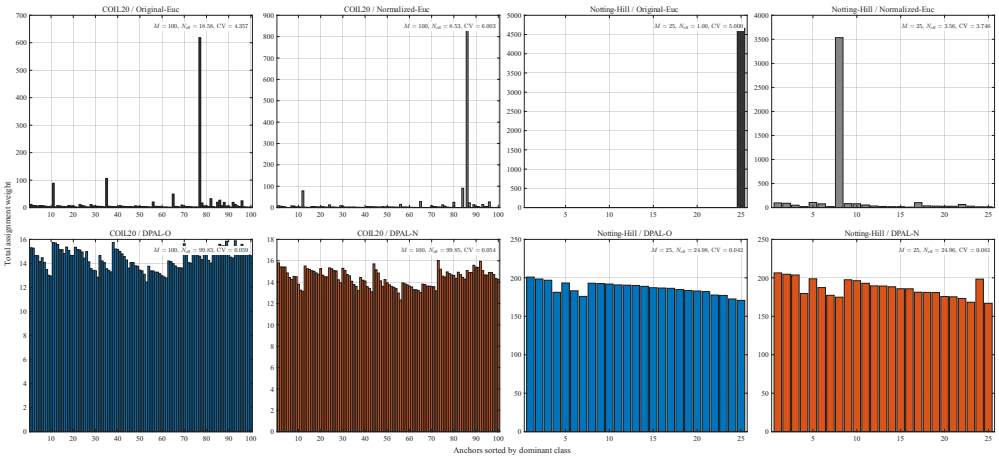

Figure 10: Anchor-usage distributions of the four controlled variants on COIL20 and Notting-Hill.

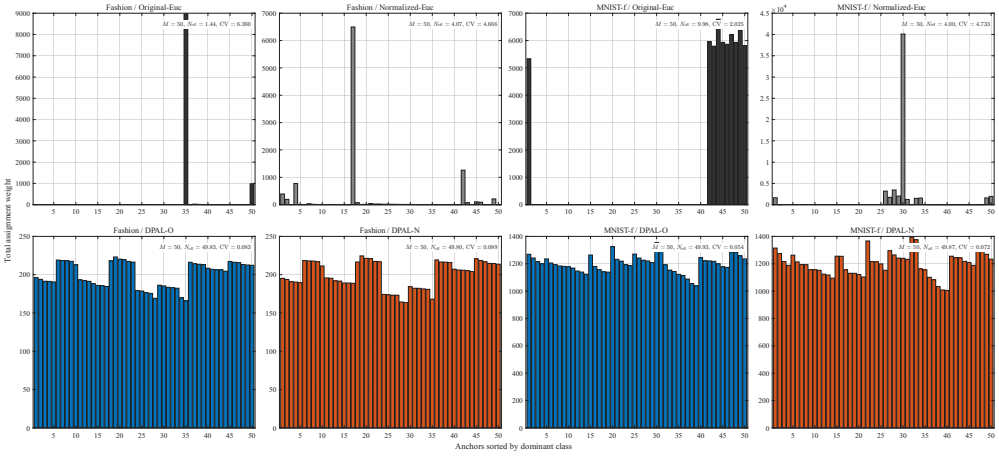

Figure 11: Anchor-usage distributions of the four controlled variants on Fashion and MNIST-f.

Taken together, these results further explain the anchor-number sensitivity observed in Figure 4. Under Euclidean reconstruction, the assignment norm participates in fitting the reconstruction scale. Consequently, increasing the number of available anchors does not necessarily produce a corresponding expansion of the learned representation; the assignments can remain concentrated on a small subset of anchors even for large M. DPAL removes the assignment-norm effect from the reconstruction loss and makes broader use of the available anchor set as M increases, allowing the learned representation to adapt more consistently across anchor settings.

B Additional Comparison with Parameter-Free Methods

This supplementary experiment compares DPAL with three representative parameter-free or coefficient-free scalable multi-view clustering methods: one-pass multi-view clustering (OPMC) (Liu et al., 2021), fast parameter-free multi-view subspace clustering with consensus anchor guidance (FPMVS-CAG) (Wang et al., 2022b), and efficient one-pass multi-view subspace clustering with consensus anchors (EOMSC-CA) (Liu et al., 2022). These methods form a particularly relevant comparison group because their objectives do not require a dataset-specific continuous regularization trade-off coefficient. Likewise, DPAL changes the reconstruction geometry without introducing an additional balancing coefficient.

B.1 Experimental Protocol

All methods are evaluated on the same ten datasets under both the original and sample-wise ℓ_2-normalized inputs. We use the released implementations and follow the settings recommended in the corresponding papers. As in the main experiment, the better input is reported for each competing method, whereas DPAL-O and DPAL-N are shown separately. We report ACC and NMI in percentage.

Table 4: Clustering results (%) of the parameter-free methods. ACC and NMI are reported as mean±standard deviation on separate rows. For competing methods, superscripts O and N denote original and normalized inputs, respectively. The best result is in bold.

Dataset	Metric	OPMC	FPMVS-CAG	EOMSC-CA	DPAL-O	DPAL-N
3Sources	ACC	$47.91 \pm 5.22^{\mathrm{N}}$	$26.63 \pm 0.00^{\mathrm{N}}$	$36.69 \pm 0.00^{\mathrm{N}}$	$\mathbf{86.24 \pm 4.44}$	82.19 ± 4.63
	NMI	$33.92 \pm 6.80^{\mathrm{N}}$	$5.41 \pm 0.00^{\mathrm{N}}$	$17.21 \pm 0.00^{\mathrm{N}}$	$\mathbf{76.01 \pm 3.30}$	73.84 ± 2.72
BBCSport	ACC	$68.85 \pm 8.62^{\mathrm{N}}$	$42.10 \pm 0.00^{\mathrm{O}}$	$46.32 \pm 0.00^{\mathrm{O}}$	$\mathbf{94.81 \pm 0.35}$	94.23 ± 0.82
	NMI	$57.73 \pm 9.01^{\mathrm{N}}$	$15.09 \pm 0.00^{\mathrm{O}}$	$21.73 \pm 0.00^{\mathrm{O}}$	$\mathbf{85.44 \pm 0.90}$	84.30 ± 1.24
MSRC	ACC	$73.52 \pm 8.91^{\mathrm{N}}$	$78.57 \pm 0.00^{\mathrm{O}}$	$67.14 \pm 0.00^{\mathrm{O}}$	59.10 ± 1.53	$\mathbf{87.79 \pm 0.23}$
	NMI	$67.86 \pm 5.63^{\mathrm{N}}$	$68.56 \pm 0.00^{\mathrm{O}}$	$56.08 \pm 0.00^{\mathrm{O}}$	47.15 ± 1.43	$\mathbf{78.45 \pm 0.44}$
Fashion	ACC	$65.74 \pm 6.21^{\mathrm{N}}$	$60.34 \pm 4.94^{\mathrm{O}}$	$68.77 \pm 0.00^{\mathrm{N}}$	$\mathbf{82.29 \pm 1.05}$	81.90 ± 1.97
	NMI	$76.54 \pm 3.24^{\mathrm{N}}$	$69.70 \pm 3.57^{\mathrm{O}}$	$\mathbf{80.13 \pm 0.00}^{\mathrm{N}}$	78.96 ± 0.44	79.96 ± 0.60
Notting-Hill	ACC	$80.85 \pm 8.92^{\mathrm{N}}$	$71.31 \pm 0.00^{\mathrm{O}}$	$86.74 \pm 0.00^{\mathrm{N}}$	85.33 ± 2.26	$\mathbf{94.78 \pm 2.43}$
	NMI	$79.16 \pm 6.15^{\mathrm{N}}$	$67.72 \pm 0.00^{\mathrm{O}}$	$73.66 \pm 0.00^{\mathrm{N}}$	76.48 ± 2.59	$\mathbf{90.21 \pm 3.43}$
NGs	ACC	$87.59 \pm 10.30^{\mathrm{N}}$	$73.80 \pm 0.00^{\mathrm{O}}$	$68.60 \pm 0.00^{\mathrm{N}}$	96.90 ± 0.45	$\mathbf{98.25 \pm 0.24}$
	NMI	$77.81 \pm 9.34^{\mathrm{N}}$	$59.23 \pm 0.00^{\mathrm{O}}$	$60.95 \pm 0.00^{\mathrm{N}}$	90.59 ± 1.19	$\mathbf{94.32 \pm 0.77}$
Reuters	ACC	$49.44 \pm 4.23^{\mathrm{N}}$	$44.33 \pm 0.00^{\mathrm{O}}$	$46.50 \pm 0.00^{\mathrm{N}}$	64.11 ± 1.11	$\mathbf{64.67 \pm 0.59}$
	NMI	$34.35 \pm 2.77^{\mathrm{N}}$	$21.28 \pm 0.00^{\mathrm{O}}$	$23.09 \pm 0.00^{\mathrm{N}}$	42.73 ± 1.00	$\mathbf{43.33 \pm 1.30}$
COIL20	ACC	$63.29 \pm 6.09^{\mathrm{O}}$	$63.46 \pm 1.50^{\mathrm{O}}$	$60.56 \pm 0.00^{\mathrm{O}}$	$\mathbf{73.54 \pm 2.32}$	70.26 ± 2.77
	NMI	$79.23 \pm 1.94^{\mathrm{O}}$	$76.24 \pm 0.52^{\mathrm{O}}$	$81.14 \pm 0.00^{\mathrm{O}}$	$\mathbf{82.04 \pm 1.25}$	79.62 ± 1.26
Wiki	ACC	$57.99 \pm 2.03^{\mathrm{N}}$	$29.42 \pm 1.45^{\mathrm{O}}$	$56.35 \pm 0.00^{\mathrm{N}}$	$\mathbf{60.62 \pm 0.16}$	58.93 ± 0.44
	NMI	$54.67 \pm 0.45^{\mathrm{N}}$	$15.56 \pm 0.96^{\mathrm{O}}$	$53.92 \pm 0.00^{\mathrm{N}}$	$\mathbf{54.98 \pm 0.18}$	50.72 ± 0.14
MNIST-f	ACC	$92.05 \pm 7.04^{\mathrm{N}}$	$84.99 \pm 7.40^{\mathrm{O}}$	$98.30 \pm 0.00^{\mathrm{N}}$	$\mathbf{99.04 \pm 0.00}$	98.58 ± 0.00
	NMI	$92.81 \pm 2.49^{\mathrm{N}}$	$91.74 \pm 2.70^{\mathrm{O}}$	$95.22 \pm 0.00^{\mathrm{N}}$	$\mathbf{97.06 \pm 0.00}$	95.98 ± 0.00

B.2 Results and Discussion

Table 4 shows that DPAL achieves the best ACC on all ten datasets and the best NMI on nine datasets. On Fashion, EOMSC-CA obtains a slightly higher NMI, while DPAL retains a clearly higher ACC. Overall, DPAL demonstrates strong performance among the parameter-free methods across the ten benchmarks.

C Additional Anchor-Number Diagnostics

Figure 12 completes the anchor-number sensitivity study in Figure 4 with the two remaining benchmarks, MSRC and Wiki. Only settings that satisfy the strict orthogonality constraint are shown.

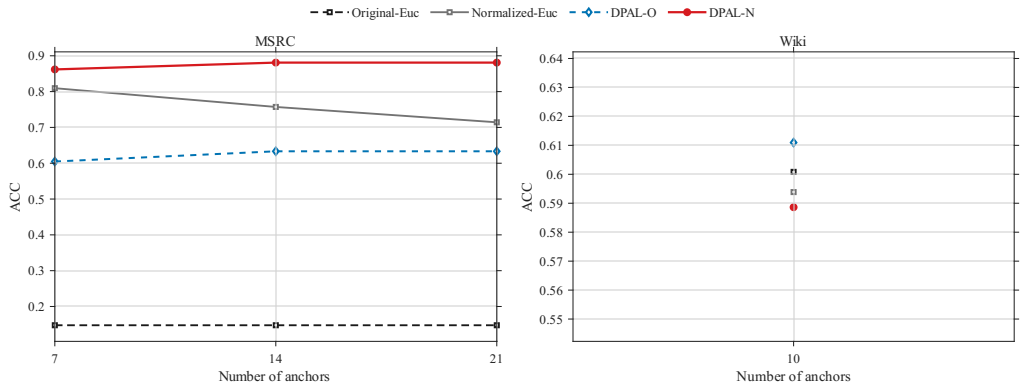

Figure 12: ACC versus the number of anchors for the four controlled variants on MSRC and Wiki.

Figure 13 supplements the assignment-norm diagnostic in Figure 5 with Fashion, MNIST-f, and Wiki. For Wiki, the smallest view dimension equals the number of classes ($d_{\min} = k = 10$), so strict orthogonality permits only $M = 10$ ($m = 1$); the single feasible setting is therefore reported rather than extrapolated.

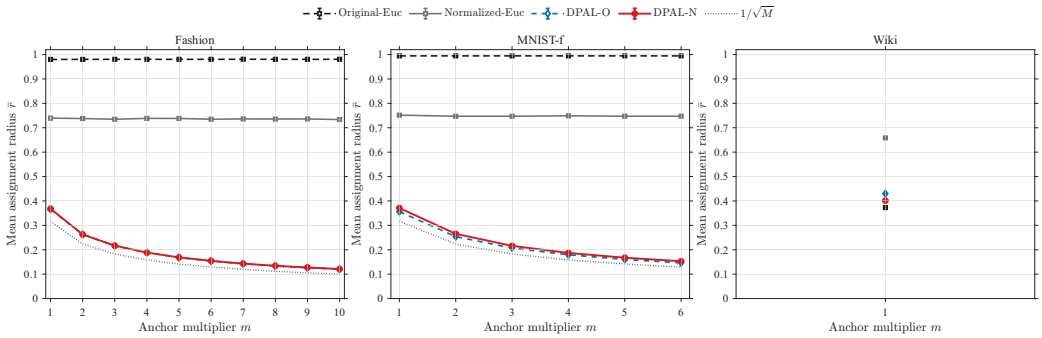

Figure 13: Mean assignment radius versus the anchor multiplier for the four controlled variants on Fashion, MNIST-f, and Wiki. The dotted curve denotes the theoretical lower bound $1/\sqrt{M}$.